ANTIOXIDANTS & REDOX SIGNALING
Volume 14, Number 4, 2011

DOI: 10.1089/ars.2010.3207

ORIGINAL RESEARCH COMMUNICATION

Glucose-6-Phosphate Dehydrogenase Is a Regulator of Vascular Smooth Muscle Contraction

Rakhee S. Gupte,[1] Hirotaka Ata,[1] Dhawjbahadur Rawat,[1] Madoka Abe,[1] Mark S. Taylor,[2] Rikuo Ochi,[1] and Sachin A. Gupte[1]

Abstract

Glucose-6-phosphate dehydrogenase (G6PD) is the rate-limiting enzyme in the pentose phosphate pathway and a major source of nicotinamide adenine dinucleotide phosphate reduced (NADPH), which regulates numerous enzymatic (including glutathione reductase and NADPH oxidase that, respectively, generates reduced glutathione and reactive oxygen species) reactions involved in various cellular actions, yet its physiological function is seldom investigated. We, however, recently showed that inhibiting G6PD causes precontracted coronary artery (CA) to relax in an endothelium-derived relaxing factor- and second messenger-independent manner. Here we assessed the role of G6PD in regulating CA contractility. Treating bovine CAs for 20 min with potassium chloride (KCl; 30 m*M*), amphotericin B (50 μM), or U46619 (100 n*M*) significantly ($p < 0.05$) increased both G6PD activity and glucose flux through the pentose phosphate pathway. The effect was Ca^{2+} independent, and there was a corresponding increase in protein kinase C (PKC) activity. Activation of G6PD by KCl was blocked by the PKCδ inhibitor rottlerin (10 μM) or by knocking down PKCδ expression using siRNA. Phorbol 12, 13-dibutyrate (10 μM), a PKC activator, significantly increased G6PD phosphorylation and activity, whereas single (S210A, T266A) and double (S210A/T266A) mutations at sites flanking the G6PD active site significantly inhibited phosphorylation, shifted the isoelectric point, and reduced enzyme activity. Knocking down G6PD decreased NADPH and reactive oxygen species generation, and reduced KCl-evoked increases in $[Ca^{2+}]_i$ and myosin light chain phosphorylation, thereby reducing CA contractility. Similarly, aortas from G6PD-deficient mice developed less KCl/phorbol 12, 13-dibutyrate-evoked force than those from their wild-type littermates. Conversely, overexpression of G6PD augmented KCl-evoked increases in $[Ca^{2+}]_i$, thereby augmenting CA contraction. Our findings demonstrate that G6PD activity and NADPH is increased in activated CA in a PKCδ-dependent manner and that G6PD modulates Ca^{2+} entry and CA contractions evoked by membrane depolarization. *Antioxid. Redox Signal*. 14, 543–558.

Introduction

Glucose-6-phosphate dehydrogenase (G6PD) is the rate-limiting enzyme that commits glucose to the pentose phosphate pathway (PPP). It is responsible for the generation of nicotinamide adenine dinucleotide phosphate reduced (NADPH), a key cofactor in various redox and antioxidant systems, and ribose 5-phosphate, an essential precursor for the *de novo* synthesis of RNA and DNA. A remarkable characteristic of G6PD is its genetic diversity. Mainly produced from missense mutations, numerous G6PD variants showing different levels of activity with diverse clinical implications have been described. It has been proposed, for example, that G6PD deficiency resulting from a highly prevalent functional polymorphism may contribute to the high incidence of coronary artery (CA) disease among African Americans, and has been associated with hypertension and diabetes mellitus (9). Conversely, epidemiological studies have associated the low rate of mortality due to ischemic heart disease and cerebrovascular disease in Sardinian males to G6PD deficiency (7, 38).

Within the cardiovascular system, G6PD-derived NADPH promotes endothelial cell growth and nitric oxide generation (29, 31) and is essential for regulation of basal and nitric oxide-stimulated soluble guanylyl cyclase activity in smooth muscle (21). G6PD-derived NADPH also fuels protein kinase C (PKC)- and angiotensin II (Ang II)-stimulated NADPH oxidase activity in CA and aorta and enhances superoxide anion generation (16, 33), which mediates Ang II-induced hypertension and aortic smooth muscle hypertrophy (33). On the

Departments of [1]Biochemistry & Molecular Biology and [2]Physiology, University of South Alabama, College of Medicine, Mobile, Alabama.

other hand, G6PD deficiency reduces vascular superoxide production and the severity of atherosclerotic lesions in ApoE$^{-/-}$ model mice (34).

Recently, we demonstrated that inhibition of G6PD leads to a reduction in the NADPH/NADP$^+$ ratio within the vasculature, lungs, and heart. This change in redox state was subsequently found to be associated with diminished arterial tone (15, 19), a reduction in pulmonary arterial pressure (19, 20), and diminished myocardial contractility (22). Conversely, G6PD activity is upregulated in the failing heart, is associated with enhanced oxidative and/or reductive stress (14, 18, 40), and is a cause of dilated cardiomyopathy (40). Although, these observations suggest an important role for G6PD and the NADPH redox balance in cardiac and vascular smooth muscle (VSM) cell metabolism and in the control of numerous signaling processes in VSM (3), the role of G6PD in regulating vascular contractile function has not been characterized. Therefore, the focus of this study was to determine (i) whether G6PD is activated in contracting smooth muscle, (ii) how is G6PD activated in stimulated CA, and (iii) whether activation of G6PD modulates contraction of CA. Our findings show that G6PD expressed in VSM cells regulates NADPH redox in VSM and modulates its contractility. This effect could have significant importance in the regulation VSM function under normal conditions and in cardiovascular diseases associated with hypertension, diabetes mellitus, and metabolic syndrome.

Materials and Methods

Methods are concisely described below. Detailed descriptions of all methods are provided separately in the Supplementary Data (available online at www.liebertonline.com/ars). Left anterior descending and circumflex CAs were harvested from bovine hearts purchased from a local slaughterhouse (Stuckey's Meat Packer). After quickly excising the heart from the animal, it was placed in normal Tyrode solution (in m*M*: 135 NaCl, 5.4 potassium chloride [KCl], 1.8 $CaCl_2$, 1.0 $MgCl_2$, 5 HEPES, and 11 glucose; pH was adjusted to 7.40 with NaOH) and transported to the laboratory on ice. Bovine CA smooth muscle cells (CASMCs) were purchased from Cell Application, Inc. All reagents used in the present study were purchased from Sigma Chemical. U46619 was obtained from Cayman Chemical.

Western blot analysis

Proteins were extracted from frozen tissue in lysis buffer, after which Western blot analysis using the specific antibodies mentioned in the individual figures was performed as described previously (16).

Detection of G6PD using immunohistochemistry

CA rings were embedded in optimum cutting temperature media and cut into 6–7 μm sections. The sections were air-dried and fixed in acetone at room temperature, after which they were incubated with polyclonal anti-G6PD antibody (1:300 dilution; Santa Cruz Biotech) overnight at 4°C, and with alkaline phosphatase-conjugated goat IgG anti-rabbit for 2 h. Images of the stained sections were collected using an Olympus Plan×10/NA 0.25 Phi objective. In each experiment, all data were collected at identical imaging settings.

G6PD activity

The activity of G6PD was measured in CA homogenates by following the reduction of NADP$^+$ to NADPH (16). NADPH fluorescence (excitation, 340 nm; emission, 460 nm) was detected using Flx800 microplate and Synergy 2 fluorescence detectors (BioTek Instruments).

NADP(H) levels

The levels of NADP(H) in CA were determined by high-performance liquid chromatography, Elite LaChrom Chromatography System from Hitachi Corporation, using previously published methods (21).

6-Phosphogluconate estimation

6-Phosphogluconate, an oxidative byproduct of the PPP, was measured in CA using a fluorometric method previously described by Kauffman *et al.* (26).

Measurement of glycolysis and glucose oxidation

Glucose metabolism in CA was determined after modifying the protocols published by Smith *et al.* (48). Briefly, endothelium- and adventitia-removed CA tissue (0.5–0.8 g) was pretreated with or without KCl (30 m*M*) and U46619 (100 n*M*) in 21%O_2–5%CO_2 for 1 h and was incubated at 37°C for 1 h in HEPES buffer, pH 7.4, containing [5-^{3}H] glucose and 1-^{14}C-glucose in the absence or presence of KCl or U46619. The resulting ^3H_2O and $^{14}CO_2$ generation from these tissues was estimated as described by Recchia *et al.* (43). The rate of glucose flux through glycolysis or the PPP was determined by ^3H_2O and $^{14}CO_2$ formation, respectively, per gram of CA tissue and the activity of these pathways in KCl and U46619 treated rings is reported as % change in the generation of ^3H_2O and $^{14}CO_2$ of the control resting rings prepared from the same CA tissue.

PKC activity

Activation of PKC in CA smooth muscle was assessed using a nonradioactive assay kit purchased from Stressgen. ELISA was performed as per the manufacturer's protocol, and activity was reported as absorbance/mg protein.

Coimmunoprecipitation studies

CA rings were pretreated with contractile agents for various time intervals indicated in the individual figures, after which they were homogenized in lysis buffer containing 1 mM Na_3VO_4 and 1 mM NaF, as described previously (12). The precleared lysates were incubated with polyclonal anti-G6PD antibody (Sigma) or polyclonal anti-phosphoSer PKC substrate-specific antibody (Cell Signaling) for 3 h at 4°C. The immunocomplexes were then immobilized on agarose-A and G beads overnight at 4°C. Western blot analysis was then carried out as described previously and specific proteins were detected using chemiluminescence.

PKCδ and G6PD knockdown in CA

After incubation in DMEM in a 24-well plate overnight at 37°C, CA rings (300 μm) were transfected with smartpool

siRNA (100 n*M*) targeting PKCδ or G6PD (Dharmacon) for 67 h using 10 μg of Lipofectamine 2000 reagent (Invitrogen). Control experiments were performed using a nontargeting (NT)/scrambled siRNA (negative control).

Overexpression of G6PD in HEK 293T17 cells

Human full-length G6PD cDNA cloned into the pCMV6-XL5 vector was purchased from Origene Technologies, Inc. The 1638-bp full-length/wild-type cDNA sequence of G6PD (NM_000402.3) was isolated by polymerase chain reaction, and cloned into the p-Ds-RedN1 expression vector (Clontech) between the *Nhe*I and *Xho*I sites (G6PD-RFP-wt). Single (S210A or T266A) and double (S210A/T266A) site-directed G6PD-Red-wt mutants were constructed using a Quikchange Multi Site-Directed Mutagenesis kit (Stratagene). HEK 293T17 cells (10^6) were plated in 24-well plates for 48 h and then transfected with (i) PKCδ-siRNA alone, G6PD-RFP-wt alone, PKCδ-siRNA+0.8 μg of p-Ds-Red, or PKCδ-siRNA+G6PD-RFP-wt; or (ii) 0.8 μg of p-Ds-Red, G6PD-RFP-wt, G6PD-RFP-S, G6PD-RFP-T, or G6PD-RFP-ST using 2 μg of FUGENE 6 reagent (Roche) for 48 h.

Construction of G6PD-coral green fluorescent protein chimera in adenoviral vector and transfection in bovine coronary artery

The 1638 bp full-length/wild-type cDNA sequence of G6PD was isolated by polymerase chain reaction as mentioned above and then cloned into a pshuttle-CMV adenoviral (AD) vector (Genscript), between *Sal*I/*Hin*dIII restriction sites such that it had a coral green fluorescent protein (cGFP) gene fused at its C-terminus. Five micrograms of adenoviral G6PD-wt-cGFP was transfected in bovine coronary artery (BCA) using 20.0 μg of Lipofectamine 2000 as described previously for 48 h.

2D electrophoresis

Immunoprecipitation of CA (3–4 mm) rings was carried out as described above. The beads were washed several times and stored at −80°C overnight. HEK 293T17-cells were transiently transfected with either G6PD-RFP-Wt or G6PD-RFP-ST, lysed in lysis buffer, and stored at −80°C overnight. The samples were sent for 2D electrophoretic analysis at the University of Illinois, Protein Sciences Facilities, Urban, IL.

Intracellular Ca^{2+} measurements

Changes in $[Ca^{2+}]_i$ levels were determined in CA using Fluo-4 or Ca^{2+} green (6, 28). To achieve a higher time resolution, changes in Ca^{2+} fluorescence were determined based on excitation at a single wavelength, and expressed as the ratio of the time-resolved fluorescence variation from the basal fluorescence (at 480 nm; $f_{480/520}$). Ca^{2+} concentrations were determined from the Fura 3PE 340 nm/380 nm fluorescence ratio as previously described (15).

Contraction of CA

Isolated, endothelium-intact left anterior descending CA rings were prepared from bovine hearts and studied for changes in isometric force, as described previously (15).

Myosin phosphatase target subunit 1 and myosin light chain phosphorylation

The phosphorylation status of myosin phosphatase target subunit 1 (MYPT1) at T855, which is phosphorylated by Rho kinase (52), in CA was determined by Western blot analysis using anti-phospho-MYPT1 antibodies (Cell Signaling), whereas myosin light chain (MLC) at S20 in CA was determined as previously described (36).

In vitro *phosphorylation*

Immunoprecipitation of CA (3–4 mm) rings were performed as described above using polyclonal anti-G6PD antibody (for BCA) and polyclonal anti-RFP antibody (for 293 cells), respectively, for 4 h at 4°C followed by immobilizing the immunocomplexes on agarose-A and G beads overnight at 4°C. *In vitro* phosphorylation assays were carried out in a 50 μl reaction mixture containing the kinase buffer (in m*M*; 5 3-(N-morpholino)propane sulfonic acid, 2.5 β-glycerophosphate, 1 ethylene glycol tetraacetic acid, 0.4 ethylene diaminetetraacetic acid, 5 $MgCl_2$, 0.05 dithiothreitol, 0.1 $CaCl_2$, 0.18 ATP, 0.05 mg/ml phosphatidylserine, pH 7.2), 100 ng of PKCδ (Cell Signaling), and 20 μl of the respective beads at room temperature for 30 min. The reactions were terminated by the addition of 2×sodium dodecyl sulfate sample buffer and boiling at 95°C for 10 min. Phosphorylation of endogenous G6PD and ectopically expressed G6PD-RFP proteins (wild type and site directed mutagenesis) was determined by immunoblotting with anti-phospho-(Ser) PKC substrate antibody as described by Jones *et al.* (25) as well as with anti-G6PD (BCA) and anti-RFP (293) antibodies, respectively, to confirm the pull-down of the respective proteins. Three hundred nanograms of histone 2B (H2B; New England Biolabs) and heat-shock protein 20 (a kind gift from Dr. Gerthoffer, University of South Alabama, Mobile, AL) was used as positive and negative controls for PKCδ phosphorylation, and immunoblotting for these substrates were performed using monoclonal anti-H2B (Cell signaling) and polyclonal anti-heat-shock protein 20 (Stressgen) antibodies, respectively.

Detection of reactive oxygen species

Reactive oxygen species (ROS) such as O_2^- was determined by dihydroethidium staining procedure (13). Breifly, groups of CA rings prepared as described for the force generation studies were incubated for 30 min at 37°C with dihydroethidium (5 μ*M*) in relaxing solution and were then contracted with KCl (30 m*M*). The CA rings were quickly removed from the wire hooks and then embedded in optimum cutting temperature media and frozen in liquid nitrogen. Cryosections (5-μm-thick cross sections) were then cut, fixed in acetone, air–dried, and mounted in Aquamount (Vector Laboratories) at room temperature. Tissue samples were excited with 480 nm and emission spectra were recorded at 567 nm. Image data were collected using a Leica Plan 63xAPO 0.25 Phi objective. All data were collected at identical imaging settings.

Glutathione reductase activity

Glutathione reductase activity was measured in CA homogenates using a kit purchased from Cayman Chemical

Co. as described previously (13). Reduction in NADPH fluorescence was detected using a Flx800 microplate and Synergy 2 fluorescence detectors (excitation, 340 nm; emission, 460 nm; BioTek Instruments).

Statistical analysis

Values are mean ± standard error. ANOVA and *post hoc* Fisher's protected *t*-test were used for analysis of all studies of vascular contractility. All enzyme activity and Western blot data were analyzed using Student's *t*-tests. Values of $p < 0.05$ were considered significant. In all cases, the number of experimental determinations (n) was equal to the number of hearts from which CAs were harvested for this study.

Results

G6PD is activated by membrane depolarization and stimulation of G protein-coupled receptors in bovine CASMCs and CA

To determine whether G6PD is involved in regulating VSM contraction, we tested whether the enzyme is activated by KCl or U46619. Western blot (Fig. 1A) and immunohistochemical (Fig. 1B) analyses showed that G6PD is expressed in both the CA and CASMCs, and that the enzyme is active (Fig. 1C). The G6PD activity in CA was increased 1.5- to 2.0-fold by stimulating the tissue with KCl (30 m*M*), which depolarizes the cell membrane, or U46619 (100 n*M*), a G protein-coupled receptor (GPCR) agonist (Fig. 1D), leading to significant increases in both 6-phosphogluconate (Fig. 1E) and NADPH (Fig. 1F), and

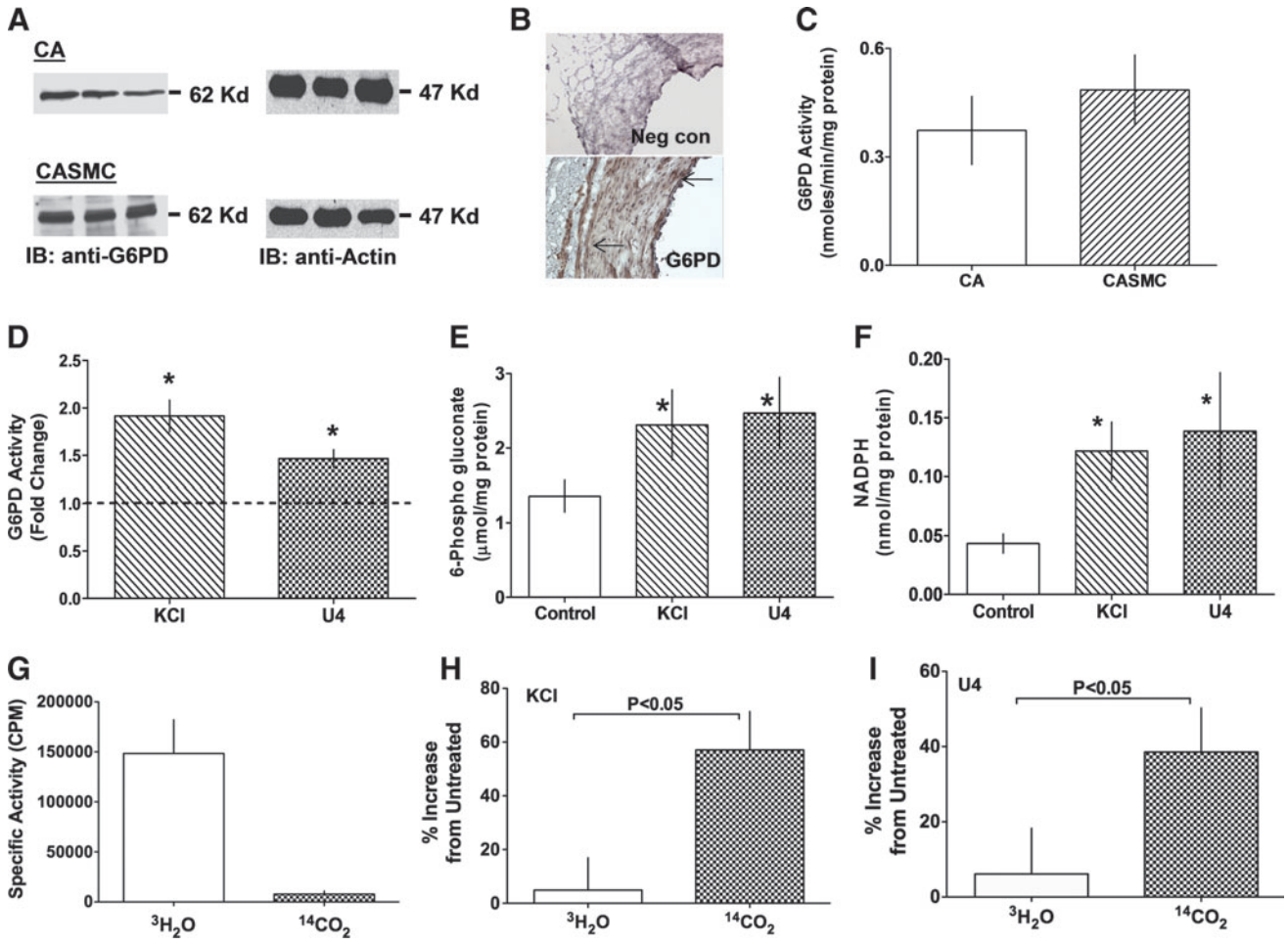

FIG. 1. Activation of G6PD by KCl and U46619. (A) Western blot analysis of G6PD expression in extracts from three bovine CAs and three cultured bovine CASMCs separately loaded in each lane (blots are representative of eight such experiments). **(B)** Immunohistochemical analyses of G6PD expression in CAs (magnification 20×; images are representative of four similar experiments). *Arrows* indicate brown positive staining in tunica intima and media. **(C)** G6PD activity determined in endothelium-intact CA ($n = 30$) and CASMCs ($n = 15$). Levels of G6PD activity **(D)**, 6-phosphogluconate **(E)**, and NADPH **(F)** increased from baseline in CA treated for 20 min with KCl (30 m*M*; $n = 25$) or U46619 (100 n*M*; $n = 25$). Glucose is metabolized through glycolysis in resting CA (**G;** $n = 8$), but glucose flux through the pentose phosphate pathway increased upon stimulation of CA by KCl **(H)** or U46619 **(I)**. *$p < 0.05$. CA, coronary artery; G6PD, glucose-6-phosphate dehydrogenase; KCl, potassium chloride; NADPH, nicotinamide adenine dinucleotide phosphate reduced; SMC, smooth muscle cell. (For interpretation of the references to color in this figure legend, the reader is referred to the web version of this article at www.liebertonline.com/ars).

$NADPH/NADP^+$ ratio increased ($p < 0.05$) from 1.9 to 4.2. The effects of KCl (10–90 m*M*) and U46619 (0.1–100 n*M*) on G6PD activity were dose dependent (see Supplementary Fig. S1) and were exerted within a concentration range known to evoke CA contraction. Thus, both membrane depolarization and activation of GPCR signaling appear to be involved in activating G6PD. To verify these observations, we further estimated glucose flux through glycolysis and the PPP using [5-^{3}H] glucose and [1-^{14}C] glucose, respectively. As expected, we found that glucose was predominantly metabolized through the glycolytic pathway in resting CA (Fig. 1G); however, upon stimulation of CA by KCl (Fig. 1H) or U46619 (Fig. 1I), glucose catabolism through glycolytic pathway as well as the PPP increased markedly. There was a significantly higher increase in the glucose flux through the PPP. Notably, we also found that activation of G6PD by KCl was not Ca^{2+} dependent (Fig. 2A). Consistent with that finding, application of amphotericin B (AMPB; 50 μM), an ionophore-mediating nonspecific cation permeability and membrane depolarization (1), to CAs for 20 min, also increased G6PD activity by approximately twofold (Fig. 2A).

G6PD is activated in endothelium-independent manner

Next, to determine whether G6PD activity is regulated by endothelium or endothelium-derived factors, we tested the effect of endothelium on the enzyme activity. We found that the G6PD activity was not different in endothelium-intact (0.28 ± 0.04 nmol/min/mg protein) *versus* endothelium-denuded (0.33 ± 0.09 nmol/min/mg protein) resting CAs and KCl activated G6PD to similar extent in presence (1.5-fold) or absence (1.6-fold) of endothelium.

Depolarization-induced activation of G6PD is modulated by PKC in CA

Because KCl and U46619 reportedly increase the activities of CaMKII, Rho kinase, and PKC in VSM (47, 49), we examined the possible role of signaling pathways involving these kinases in the activation of G6PD. Inhibition of Rho kinase and CaM kinase II using Y27362 (10 μM) and KN-93 (10 μM), respectively, did not block the activation of G6PD by KCl or U46619 (see Supplementary Fig. S2). On the other hand, chelerythrine (10 μM; Fig. 2B), a nonselective PKC inhibitor, and Gö6796 (10 μM; $n = 12$), an inhibitor of conventional and atypical PKC isoforms, did block activation of G6PD by KCl/U46619/AMPB, though the inhibition of KCl-induced activation by Gö6796 was less marked (KCl: 1.65 ± 0.09-fold *vs.* Gö6796 + KCl: 1.42 ± 0.54-fold; NS) than that by chelerythrine (1.21 ± 0.18-fold). We also found that phorbol 12, 13-dibutyrate (PDBu) (10 μM), a membrane-permeant PKC activator, nearly tripled G6PD activity in CA rings, and that this effect was blocked by chelerythrine (Fig. 2B). This led us to determine whether PKC is activated by membrane depolarization. Consistent with that idea, KCl, AMPB, U46619, and PDBu all significantly increased PKC activity (Fig. 2C), and pretreatment of CA with chelerythrine or rottlerin (10 μM), a selective PKCδ inhibitor, suppressed PKC activation evoked by both PDBu (by 99%) and AMPB (by 85%) as well as contraction elicited by KCl, U46619, and PDBu (see Supplementary Fig. S3).

PKCδ interacts with G6PD and increases its activity in stimulated CA

Because activation of PKC by AMPB was significantly inhibited by rottlerin, and because PKCδ is expressed in CA and CASMCs (see Supplementary Fig. S3), we tested the possibility that PKCδ modulates G6PD activity. Application of KCl (30 m*M*) to CAs for 0–20 min resulted in a triphasic response wherein the interaction of PKCδ with G6PD (as determined in coimmunoprecipitation experiments using anti-G6PD antibody) peaked within 2 min, after which there was a transient drop lasting between 2 and 5 min and then a second peak that remained stable for 10–20 min (Fig. 3A). By contrast, when CAs were treated with U46619 (100 n*M*), interaction of PKCδ with G6PD was first noted at 10 min and remained stable thereafter (Fig. 3B). Activation of G6PD by KCl (Fig. 3C) and U46619 (Fig. 3D) followed the same time course as the interaction between G6PD and PKCδ, which suggests that phosphorylation of G6PD by PKCδ is instrumental for activation of G6PD in KCl- and U46619-treated CA rings.

Additional corroborative evidence was obtained by inhibiting PKC activity using rottlerin or by knocking down endogenous PKCδ expression in CA rings. We found that rottlerin

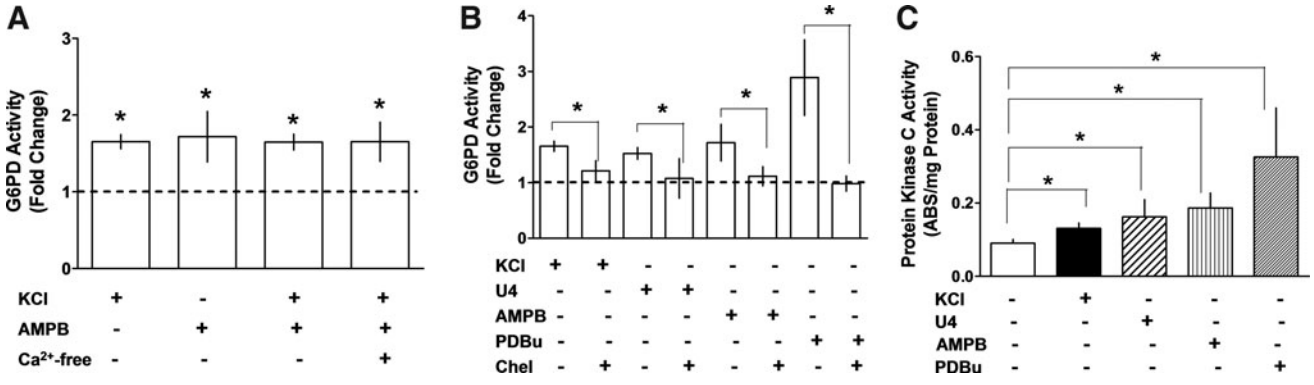

FIG. 2. Depolarization-induced activation of G6PD is mediated by PKC. (A) Application of AMPB (50 μM; $n = 10$) or KCl (30 m*M*; $n = 15$) to CA for 20 min increased G6PD activity in a Ca^{2+}-independent manner. **(B)** Activation of G6PD by KCl (30 m*M*; $n = 10$), U46619 (100 n*M*; $n = 8$), AMPB (50 μM; $n = 5$), and PDBu (10 μM; $n = 15$) was inhibited by Chel (10 μM; $n = 8$). **(C)** PKC activity is increased in CA by KCl ($n = 10$), U46619 ($n = 5$), AMPB ($n = 5$), and PDBu ($n = 7$). *$p < 0.05$. AMPB, amphotericin B; Chel, chelerytherine; PDBu, phorbol 12, 13-dibutyrate; PKC, protein kinase C.

significantly diminished G6PD activity elicited by KCl (2 min; Fig. 3E) or U46619 (20 min; Fig. 3F). In addition, immunoprecipitation of proteins phosphorylated by PKC from CA lysates using anti-phosphoserine PKC substrate-specific antibody (anti-PS-PKC substrate) (27) that recognizes PKC substrates like H2B (Fig. 3G), and Western blot analyses with anti-G6PD antibody showed that G6PD phosphorylation was greater in CAs treated with KCl or PDBu than in resting CAs (Fig. 3H). Conversely, PKCδ knockdown (Fig. 3I) significantly reduced G6PD activation otherwise elicited by KCl (30 m*M*; 20 min; Fig. 3J).

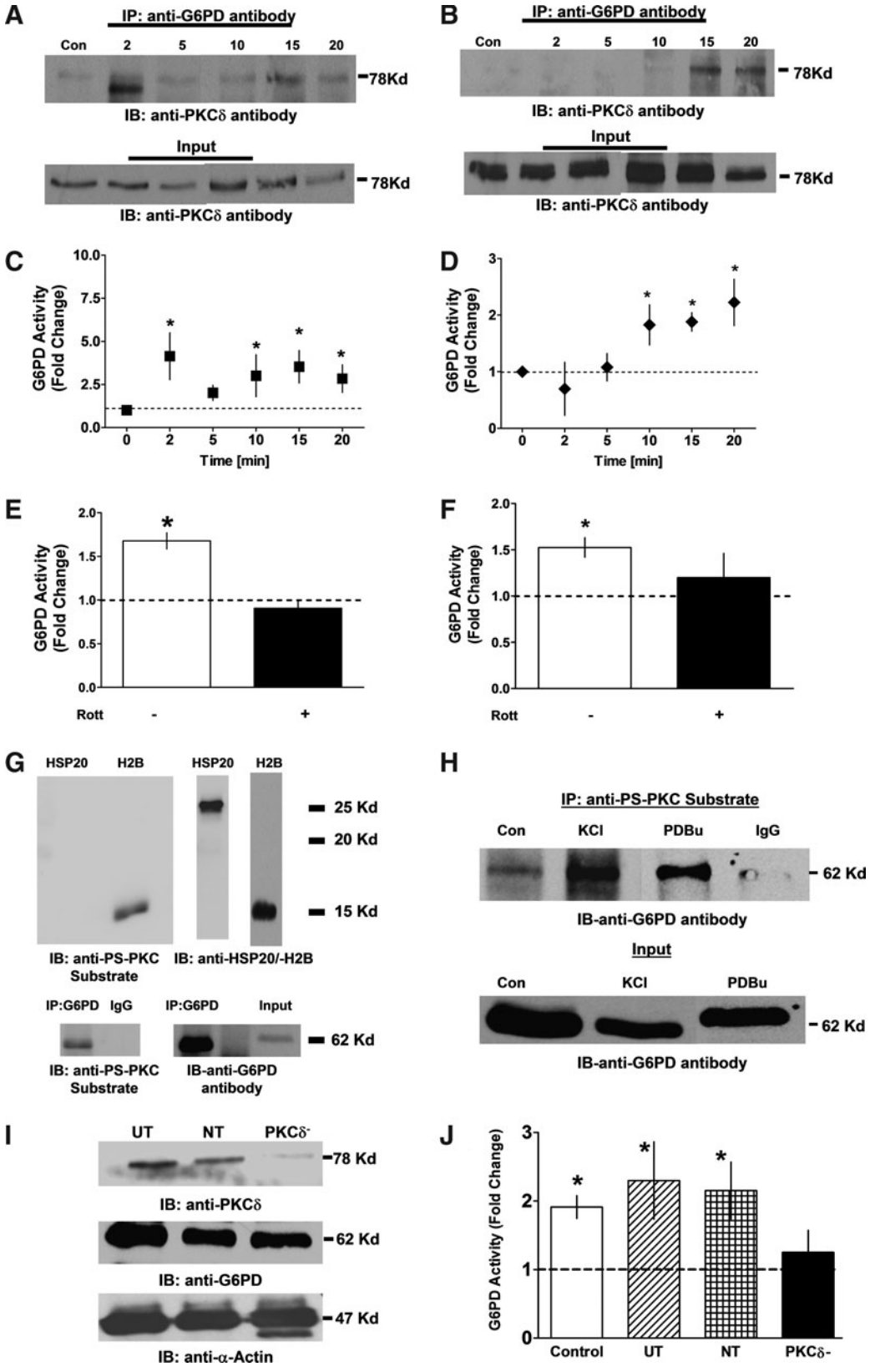

Phosphorylation of G6PD by PKCδ at S210 and T266 is essential for its activation

To substantiate our finding that phosphorylation by PKCδ is required for G6PD activation, we transfected HEK 293T17 cells with G6PD-RFP-wt alone, RFP vector+PKCδ-siRNA, or G6PD-RFP-wt+PKCδ-siRNA, and then carried out immunoprecipitation assays using anti-phosphoserine PKC substrate antibody and Western blotting with anti-G6PD antibody. We found that G6PD-RFP-wt was immunoprecipitated by the PKC substrate-specific anti-phosphoserine antibody, indicating that G6PD was phosphorylated by PKC on a serine residue (Fig. 4A-i), and that there was a concomitant >25-fold increase in the G6PD activity (Fig. 4A-ii). Moreover, knocking down endogenous PKCδ inhibited G6PD activity by 86% and abolished its immunoprecipitation.

We next overexpressed G6PD-RFP-wt (Fig. 4B-i) in HEK 293T17 cells and confirmed its expression using immunofluorescence microscopy (Fig. 4B-ii) and Western blot analysis (Fig. 4B-iii). To identify the residues crucial for PKC phosphorylation and G6PD activity, out of five PKC consenuses phosphorylation sites we substituted the serine and threonine residues in the PKC consensus sequence flanking the G6PD active site, and constructed two single (S210A = S and T266A = T) and one double (S210A/T266A = ST) G6PD mutants (note that the wild-type and mutant enzymes were similarly expressed) (Fig. 4B). To examine whether PKCδ phosphorylates G6PD, we immunoprecipitated G6PD-RFP-wt or G6PD-RFP-S, -T, and -ST mutants with anti-RFP antibody and performed *in vitro* phosphorylation using PKCδ. Western blot analysis performed with anti-PS-PKC antibody indicates that PKCδ phosphorylated G6PD (Fig. 4C-i). Then, using G6PD-RFP-wt or G6PD-RFP-ST expressed in the cells, we examined the cell lysates to determine if PKC phosphorylates G6PD *in vivo* using 2D electrophoresis. We found that G6PD-RFP-wt was phosphorylated by PKC, causing a leftward shift from alkaline to acidic pH, which was not seen with G6PD-RFP-ST (Fig. 4C-ii; indicated in a box). This suggests that both S210 and T266 are crucial for PKC phosphorylation and G6PD activity. We also measured G6PD activity and found that mutation at PKC phosphorylation sites not only reduced basal G6PD activity (Fig. 4C-iii) but also blocked the activation of G6PD otherwise seen after 2 min of stimulation with KCl (30 m*M*; Fig. 4C-iv).

Catalase inhibits PKC-dependent activation of G6PD in CA

Because PKC also activates NADPH oxidase and increases O_2^- and H_2O_2, which activates G6PD (8, 17), we examined the possible role of H_2O_2 in activating G6PD. Pretreatment of CA with peg-catalase (300 U/ml; $n = 8$) for 30 min before treating it with KCl or PDBu not only blocked but also decreased ($p < 0.05$) KCl- and PDBu-induced increase in G6PD activity (KCl: 1.8 ± 0.1 *vs.* catalase+KCl: 1.3 ± 0.1 and PDBu: 2.2 ± 0.2 *vs.* catalase+PDBu: 1.5 ± 0.2-fold as compared to the untreated control).

Knocking down endogenous G6PD diminishes CA ROS and contractility

G6PD is a major source of NADPH in CA (16), and we found a positive correlation between NADPH levels (Fig. 5A) and force generation with G6PD activity (Fig. 5B) as well as between force and NADPH levels (Fig. 5C). Therefore, to determine the direct effect of G6PD activity on vascular motor function, we used SMART pool-siRNA to knockdown endogenous G6PD expression in CA (Fig. 6A). Targeting G6PD using siRNA significantly reduced tissue levels of both enzyme's activity (Fig. 6B) and NADPH (Fig. 6C). Since G6PD-derived NADPH fuels NADPH oxidase and regulates O_2^- levels as well as glutathione reductase activity in vascular and cardiac tissue (13, 14, 33, 46), we determined whether G6PD knockdown affects ROS generation in CAs. Silencing G6PD (Fig. 6D) did not affect glutathione reductase activity (untransfected [UT]: 278 ± 74; NT: 236 ± 60; and $G6PD^-$: 301 ± 74 nmol/min/mg protein), but significantly reduced dihydroeithidium fluorescence (Fig. 6E), indicating that it decreased ROS levels. In addition, CA rings subjected to G6PD knockdown contracted significantly less than rings treated with NT siRNA or UT control rings when incubated with KCl (30 m*M*; Fig. 6F), U46619 (100 n*M*; Fig. 6G), or PDBu (10 μ*M*; Fig. 6H).

Silencing G6PD reduces KCl-induced Ca^{2+} entry, the rise in global $[Ca^{2+}]_i$, and phosphorylation of MYPT1 and MLC

To investigate how G6PD affects CA contraction, we examined the effect of G6PD knockdown on basal and KCl-induced Ca^{2+} levels in CA. G6PD knockdown significantly suppressed KCl-induced increases in CASMC $[Ca^{2+}]_i$, as compared to CAs treated with NT siRNA (Fig. 7A, D). Consistent with that finding, knocking down G6PD also reduced the rise in global $[Ca^{2+}]_i$ evoked by KCl (Fig. 7E). In addition, we found that KCl-induced phosphorylation of MYPT1 at T855 and MLC at S20 was reduced in CA rings treated with G6PD siRNA (Fig. 7F). Finally, to determine whether G6PD affects contraction by regulating Ca^{2+} entry evoked by KCl, we first tested the effect of KCl (30 m*M*) on CA contractility in the absence of extracellular Ca^{2+}. In Ca^{2+}-free solution, KCl

FIG. 3. PKCδ interacts with G6PD in stimulated CA with a concomitant increase in G6PD activity. (A, B) Coimmunoprecipitation assays showing that PKCδ interacts with G6PD in a time-dependent manner after application of 30 m*M* KCl ($n = 5$) or 100 n*M* U46619 ($n = 5$). **(C, D)** Activation of G6PD followed a similar time course. **(E, F)** Application of the PKCδ inhibitor Rott (10 μ*M*) inhibited activation of G6PD. **(G)** *In vitro* phosphorylation of recombinant HSP20 (negative control), H2B (a positive control), a PKC substrate, and G6PD immunoprecipitated from CA were detected with phosphoserine antibodies specifically recognizing PKC substrates (anti-PS-PKC substrate). **(H)** Immunoprecipitation assay showing phosphorylation of G6PD after stimulation with KCl (30 m*M*; $n = 5$) or PDBu (10 min; 10 μ*M*; $n = 5$) and immunoprecipitation with anti-PS-PKC substrate. **(I)** CA rings (300 μm inner diameter) were transfected with NT (scrambled) or PKCδ-siRNA for 67 h. PKCδ siRNA transfectant CAs showed significant suppression of PKCδ expression but not expression of G6PD or α-actin, as compared to UT CAs and CAs transfected with NT siRNA. **(J)** Activation of G6PD by KCl (30 *M*; $n = 6$–15) was significantly inhibited in CAs subjected to PKCδ knockdown. *$p < 0.05$. H2B, histone 2B; HSP20, heat-shock protein 20; NT, nontargeting; Rott, rottlerin; UT, untransfected.

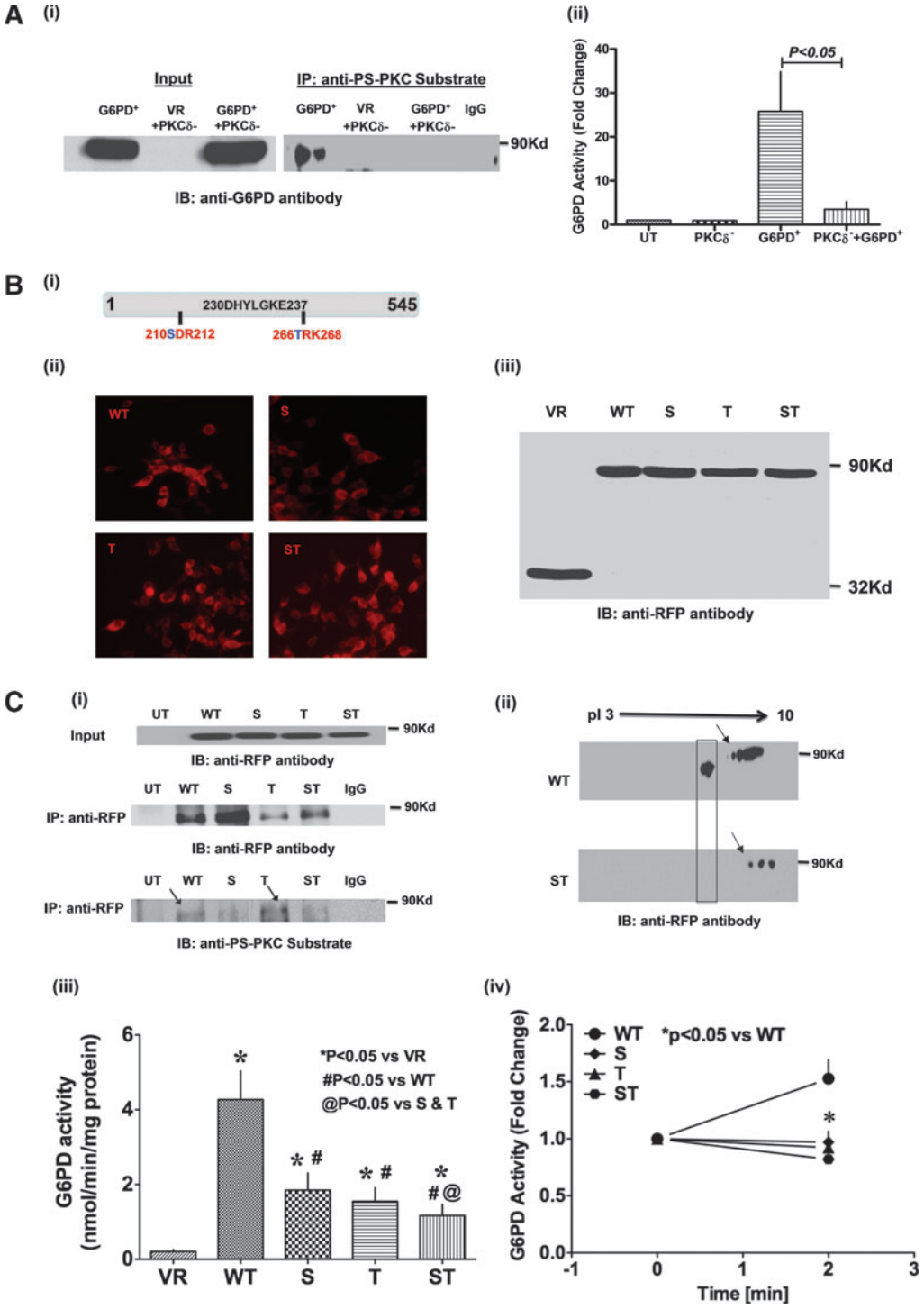

FIG. 4. Phosphorylation of S210 and T266 residues flanking the active site of G6PD by PKCδ is essential for G6PD activation. **(A-i)** Coimmunoprecipitation of ectopically overexpressed G6PD-RFP-wt with anti-phosphoserine PKC substrate antibody is abolished by silencing PKCδ (blot is representative of four experiments). Empty vector (VR) is used as a negative control. **(A-ii)** G6PD activity is significantly greater in HEK 293T17 cells expressing G6PD-RFP-wt than in UT cells ($n = 8$). Conversely, G6PD activity is significantly suppressed in HEK 293T17 cells transfected with G6PD-RFP-wt+PKCδ siRNA ($n = 4$–5). **(B)** Single (S210A, T266A) and double (S210A/T266A) mutations **(i)** were made within the PKC phosphorylation site flanking the active site of G6PD, and expression of the mutants was confirmed by immunofluorescent microscopy **(ii;** magnification: 20×) and Western blot analysis **(iii)**. **(C-i)** Western blot done with specific anti-PS-PKC substrate antibody showing *in vitro* phosphorylation by PKCδ of G6PD-RFP-wt at S210 residue. Note that the anti-PS antibody recognizes phosphorylation of T266A mutant but not the S210A and S210A/T266A mutant. **(C-ii)** Western blot after 2D electrophoresis shows that G6PD is hypophosphorylated in HEK 293T17 cells expressing the G6PD S210A/T266A double mutant (indicated by an *arrow*) and that mutating two out of five PKC phosphorylation sites abolished the leftward shift of G6PD (shown in box). **(C-iii)** Enzymatic activity was suppressed in HEK 293T17 cells expressing either a G6PD single (S210A, T266A) or double (S210A/T266A) mutant ($n = 10$–12). **(C-iv)** KCl (30 m*M*; $n = 8$)-induced increases in enzymatic activity (at 2 min) were suppressed in HEK 293T17 cells expressing one of the aforementioned G6PD mutants. (For interpretation of the references to color in this figure legend, the reader is referred to the web version of this article at www.liebertonline.com/ars).

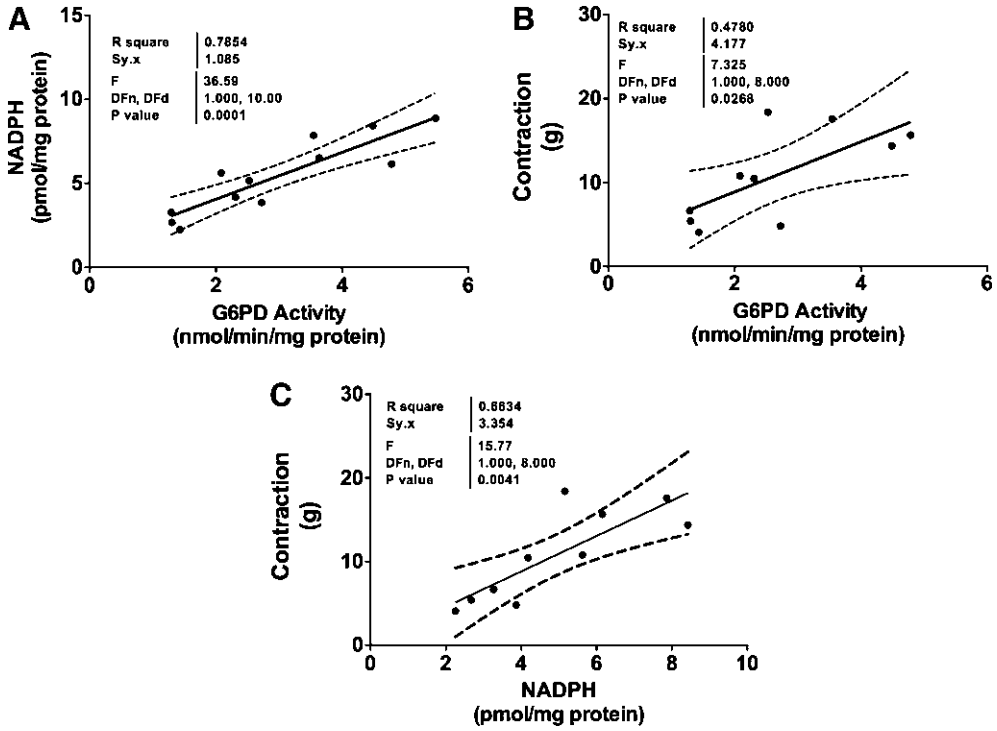

FIG. 5. G6PD is a major source of NADPH in CA. (A–C) A positive correlation between G6PD activity and NADPH levels indicate that G6PD is major source of NADPH in CA **(A)** and upon stimulation of CA with KCl (30 m*M*) G6PD activity **(B)** and NADPH levels **(C)** are increased and positively correlate with force.

did not induce contraction of CA rings. As the Ca^{2+} concentration in the bath solution was increased, the amplitudes of KCl-induced CA contractions increased correspondingly (Fig. 7G). Moreover, the contractions elicited in the knockdown rings were significantly smaller than those elicited in NT-treated rings. Knocking down G6PD also reduced ($p < 0.05$) contractions evoked by U46619 (n*M*), which acts by facilitating Ca^{2+} release from internal stores and is able to induce CA contraction in Ca^{2+}-free solution (Fig. 7H).

G6PD-deficient mice exhibit attenuated aortic contraction

G6PD-deficient ($G6PD^{def}$) transgenic mice harbor a mutation in the 5′ promoter region of the *G6PD* gene, which downregulates the gene's expression in various tissues, and decreases blood pressure and CA disease (30, 33). As expected, we found that G6PD expression (Fig. 8A) and activity (Fig. 8B) were significantly downregulated in aortas from $G6PD^{def}$ mice, as compared to those from wild-type (C3H) animals, and the contractile responses of aortas from $G6PD^{def}$ mice to KCl (30 m*M*; Fig. 8C) and PDBu (10 μM; Fig. 8D) were also attenuated.

Overexpression of G6PD increases KCl-induced rise in global $[Ca^{2+}]_i$ and contraction

Conversely, to investigate whether overexpression of G6PD increases CA contractility, we transfected the CA rings with G6PD-DNA cloned in adenovirus vector either with or without cGFP tag. CAs transfected with G6PD-DNA expressed GFP-tagged or nontagged G6PD as compared to UT controls that were cultured with transfecting reagents (Fig. 9A, B). Overexpressing G6PD increased ($p < 0.05$) KCl-evoked increases in global $[Ca^{2+}]_i$ as compared to UT controls (Fig. 9C). Consistent with these findings, overexpression of G6PD also augmented the contraction of CAs elicited by KCl and U46619 (Fig. 9D).

Discussion

Excitation–contraction (EC) coupling is a complex process involving a number of proteins and signaling pathways (49). For example, redox potential has been shown to influence the excitability of VSM (4). Barron *et al.* (3) proposed that the PPP may play an important role in VSM metabolism, and that deprivation of glucose and O_2 significantly reduces activity in the PPP. In the present study, we found that active G6PD is abundantly expressed in CASMCs, and that it is further activated by application of KCl or U46619. We also found that G6PD activation by KCl is independent of extracellular Ca^{2+}, as KCl increased G6PD activity in Ca^{2+}-free solution strongly buffered with ethylene glycol tetraacetic acid+1,2-bis(o-aminophenoxy)ethane-N, N, N, N′, N′-tetra acetic acid. Depolarization of the cell membrane using AMPB also induces Ca^{2+}-independent increases in G6PD activity in CAs, suggesting that depolarization, itself, may modulate G6PD activity in VSM (Fig. 10).

Membrane potential is an important component of EC coupling in skeletal, cardiac, and smooth muscle. Changes in membrane potential evoke conformational changes in the voltage sensing domain of voltage-gated ion channels (10), leading to the opening or closing of the channel, which in turn leads to short- or long-term changes in cell function. It now appears that membrane potential is directly sensed by other

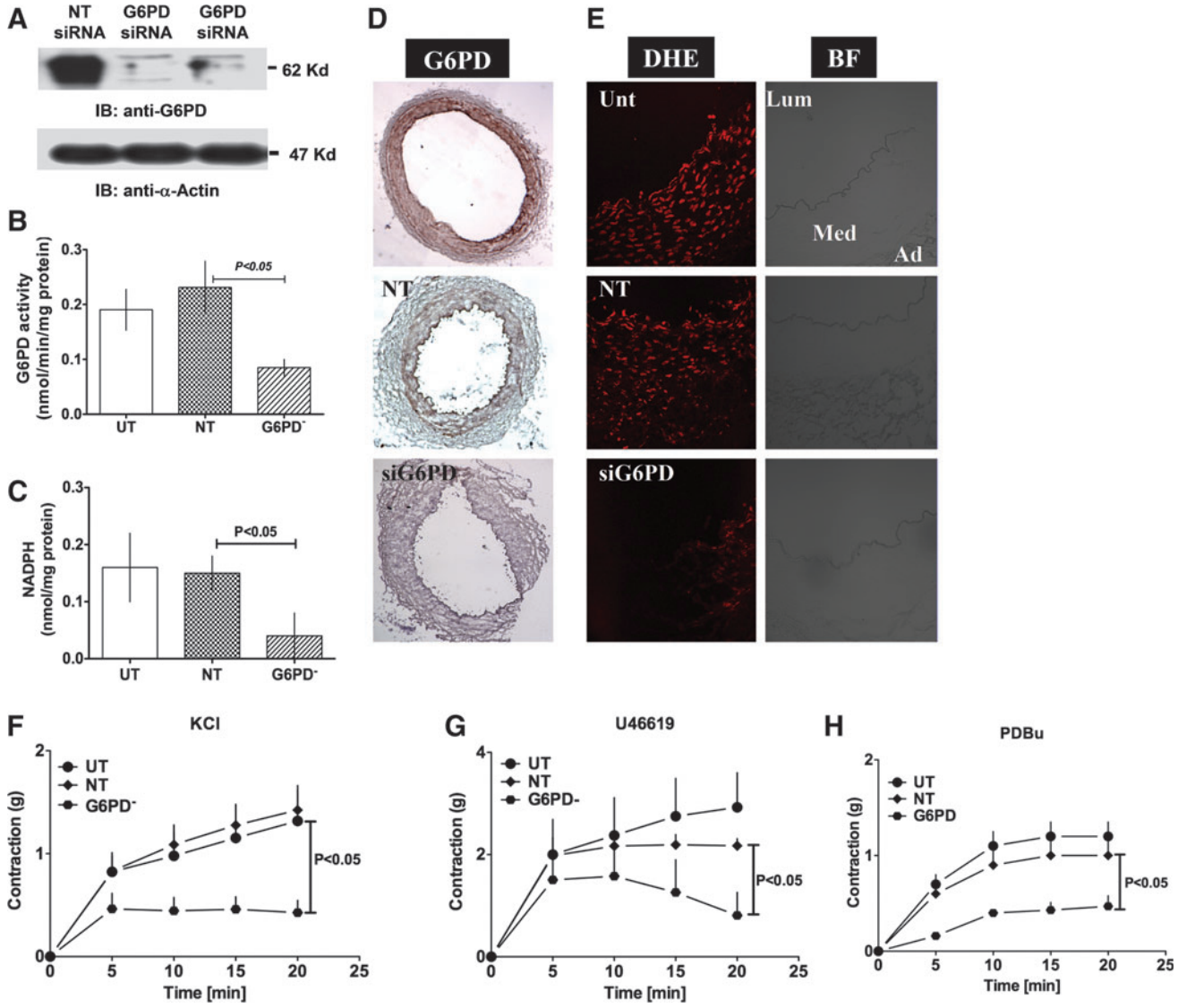

FIG. 6. G6PD knockdown reduced KCl- and U46619-induced CA contraction. (A–D) Transfection of a targeted siRNA into CAs reduced G6PD expression (**A;** blot is representative of eight experiments) and activity (**B;** $n = 8$) and NADPH levels (**C;** $n = 8$). **(D, E)** G6PD knockdown (**D;** immunohistochemistry of four experiments; magnification 4×) decreased G6PD expression and reduced superoxide levels in same tissue (**E:** representative of dichlorofluorescein fluorescence on the left & bright field on the right of four experiments; magnification: 20×oil). **(F–H)** CA contractions evoked by KCl (**F;** 30 m*M*; $n = 8$), U46619 (**G;** 100 n*M*; $n = 8$), and PDBu (**H;** 10 μM; $n = 5$) were significantly reduced by transfection with G6PD-specific siRNA, as compared to CAs transfected with NT siRNA and UT controls. Ad, adventitia; BF, bright field; DHE, dihydroeithidium; Lum, lumine; Med, media. (For interpretation of the references to color in this figure legend, the reader is referred to the web version of this article at www.liebertonline.com/ars).

types of proteins too, including phosphoinositide phosphatases, which modulates cell function through changes in the cellular diacylglycerol levels (35). For example, PKC is activated by depolarization-induced increases in Ca^{2+} and diacylglycerol (32, 42). We found that activation of G6PD by KCl or AMPB was mediated by PKC (Fig. 2C). Moreover, Gö6796, a conventional and atypical PKC isoform inhibitor, inhibited G6PD activity to a lesser degree than rottlerin, a PKCδ inhibitor (11), and than PKCδ knockdown, suggesting that activation of Ca^{2+}-independent novel or atypical PKC, more likely PKCδ, *via* membrane depolarization or by stimulation of GPCRs is, at least in part, responsible for the increase in G6PD activity seen in CA smooth muscle.

G6PD contains five classical PKC phosphorylation consensus sites (see Supplementary Data; Fig. 5) at residues 13TLR15, 210SDR212, 266TFK268, 436TKK438, and 536TYK538 (as determined from the PROSITE PROSCAN-PBIL database). Of these five sites, 210SDR212 and 266TFK268 flank the active site of G6PD (Fig. 4B-i). It is therefore plausible that phosphorylation of G6PD by PKC at these sites is necessary for its activation in CA smooth muscle. Consistent with that notion, our results suggest that G6PD is phosphorylated and its activity is significantly enhanced after treatment with KCl or PDBu. The time-dependent interaction between PKCδ and G6PD and concurrent increase in G6PD activity elicited by KCl/U46619, the inhibition of KCl/U46619-evoked activation of G6PD by

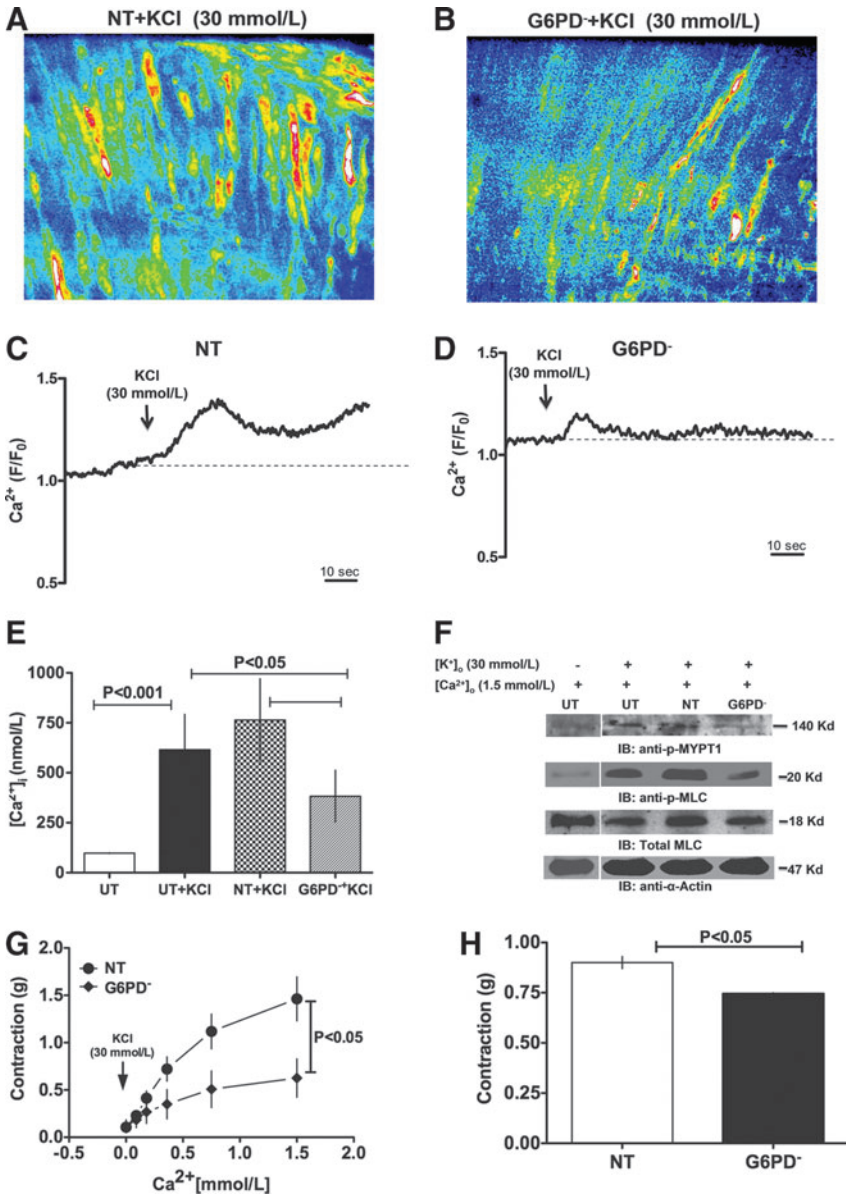

FIG. 7. G6PD knockdown decreased KCl-induced Ca^{2+} entry into CA smooth muscle. (A–D) Ca^{2+} dynamics in the smooth muscle of NT- and G6PD siRNA-treated CAs. KCl (60 m*M*)-induced Ca^{2+} entry into smooth muscle cells of CA rings transfected with NT- **(A, B)** or G6PD-siRNA **(C, D)** was evaluated based on changes in Fluo-4 fluorescence using confocal microscopy. G6PD knockdown suppressed Ca^{2+} entry into CASMCs. **(E)** G6PD knockdown suppressed KCl (30 m*M*)-induced increases in global $[Ca^{2+}]_i$ ($n = 6$) measured using Fura 3PE. **(F)** KCl (30 m*M*; 20 min)-induced phosphorylation of MYPT1 and MLC (blot is representative of three experiments). G6PD knockdown suppressed contraction of CA rings elicited by KCl (30 m*M*; $n = 5$) at the indicated extracellular Ca^{2+} concentrations **(G)** and by U46619 (100 n*M*; $n = 4$) in the absence of extracellular Ca^{2+} **(H)**. MLC, myosin light chain; MYPT1, myosin phosphatase target subunit 1. (For interpretation of the references to color in this figure legend, the reader is referred to the web version of this article at www.liebertonline.com/ars).

rottlerin, and the inhibition of KCl-induced increases in G6PD activity caused by PKCδ knockdown all suggest that PKCδ-dependent phosphorylation plays a key role in the activation of G6PD by KCl/U46619. Indeed, G6PD immunoprecipitated from CA is phosphorylated *in vitro* by PKCδ. Moreover, knocking down PKCδ in HEK 293T17 cells overexpressing G6PD significantly reduced G6PD activity. In these cells, immunoprecipitation of overexpressed G6PD with PKC substrate-specific anti-phosphoserine antibody was also abolished, suggesting that phosphorylation of S210 by PKCδ is involved in the activation of G6PD. More direct evidence was obtained from *in vitro* phosphorylation and the analysis of single (S210A, T266A) and double (S210A/T266A) G6PD mutants. These mutations within the PKC phosphorylation sequences flanking the G6PD active site reduced basal G6PD activity, blocked G6PD activation by KCl, and shifted the isoelectric point of G6PD from acidic to alkaline pH, which collectively indicate that G6PD is activated by PKC phosphorylation.

G6PD is one of the major sources of NADPH in mammalian tissue including the CA (15), and consistently a strong positive correlation between G6PD activity and NADPH levels in CA suggests that NADPH is mainly derived from the PPP. In addition, we observed a correlation between force generation and G6PD activity or NADPH levels, and found that glucose flux through the PPP shunt was significantly increased in CA stimulated by KCl or U46619, thereby indicating that activated G6PD and increased NADPH plays a role in regulating smooth muscle contractility.

Although it is well established that G6PD-derived NADPH is an essential cofactor for several oxido-reductases in vascular tissue, the effects of G6PD and the NADPH redox state on vascular function remain largely unexplored. To investigate whether G6PD or G6PD-derived NADPH redox plays a role in modulating CA contractile function, we knocked down G6PD expression by transfecting small ($\sim 300\ \mu$m) branches of the left anterior descending artery with siRNA targeting

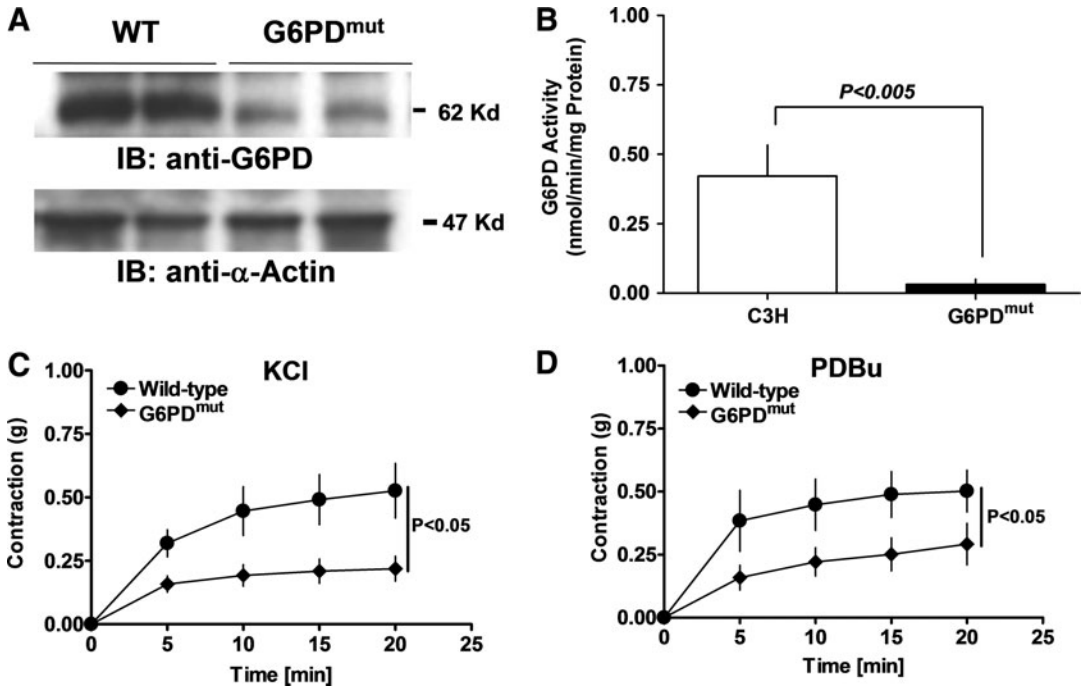

FIG. 8. G6PD-deficient mice exhibit attenuated aortic contraction. (A, B) Mutation in the 5′ promoter region of G6PD gene reduced G6PD expression (**A;** blot is representative of five experiments) and its activity (**B;** $n = 5$) in aorta. Aortas from G6PD^{def} mice developed less force in response to KCl (**C;** 30 m*M*; $n = 5$) or PDBu (**D;** 10 μM; $n = 5$) than wild-type mice. G6PD^{def}, glucose-6-phosphate dehydrogenase deficient.

G6PD, which significantly decreased G6PD expression and activity and the NADPH levels in the transfectant CAs. Further, rings of these CAs also developed significantly less isometric force upon stimulation with KCl, U46619, or PDBu than rings transfected with NT, siRNA or UT rings. Additionally, aortas from G6PD^{def} mice, which harbor a mutation in the 5′ promoter region of the G6PD gene (30), that leads to significantly reduced G6PD activity in various tissues (33), also generated less force than their wild-type littermates and age-matched controls. Collectively, these results support our hypothesis that G6PD plays a key role in force development in smooth muscle.

The effects of PPP or G6PD modulation on the mechanisms that control vascular function have not been studied.

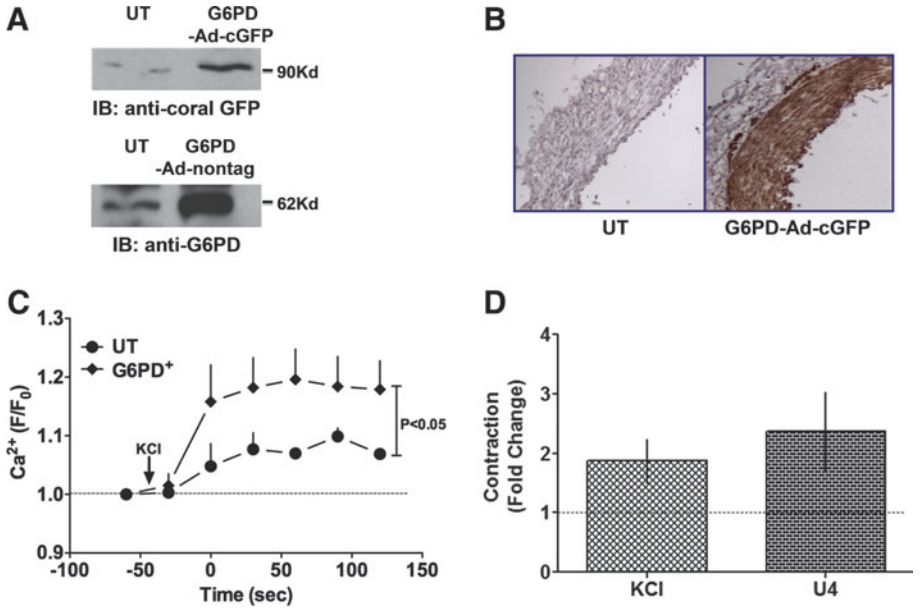

FIG. 9. G6PD overexpression increased KCl-induced Ca^{2+} entry into CA smooth muscle. (A, B) Transfection of a DNA encoding full-length G6PD increased expression of cGFP-tagged G6PD (*top*) and nontagged G6PD (*bottom*) in CAs detected by Western blotting (**A;** blot is representative of four experiments) and by immunohistochemistry (**B;** a representative of three experiments). G6PD overexpression increased Ca^{2+} entry and CA contraction. **(C)** Overexpression of G6PD increased KCl (30 m*M*)-induced increases in global $[Ca^{2+}]_i$ measured using Ca^{2+} green ($n = 5$). **(D)** Data summarizing peak contractions of CA overexpressing G6PD normalized by peak contractions of UT controls show that CA contraction evoked by KCl (30 m*M*; $n = 8$) and U46619 (100 m*M*; $n = 8$) was increased. cGFP, coral green fluorescent protein. (For interpretation of the references to color in this figure legend, the reader is referred to the web version of this article at www.liebertonline.com/ars).

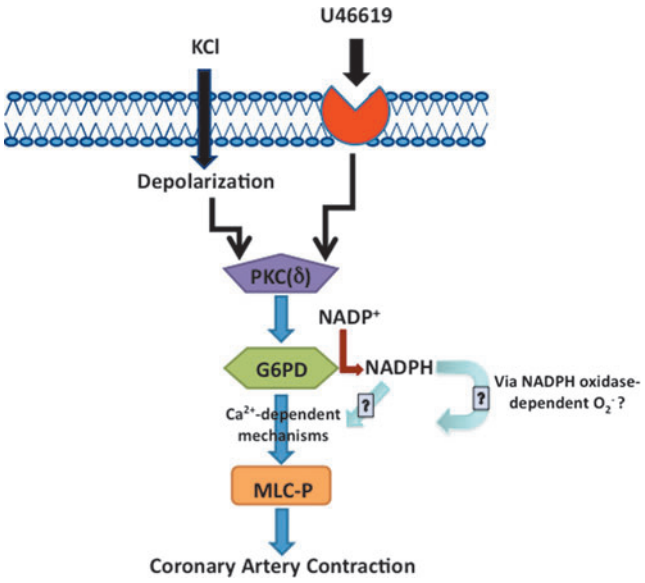

FIG. 10. A schematic diagram illustrating the role of G6PD in regulating CA contractility. A flow diagram illustrates that activation of PKC, most likely PKCδ, by depolarization or G-coupled receptors phosphorylate G6PD, and stimulated G6PD, either directly or *via* inducing changes in NADPH redox, modulates CA contraction evoked by Ca^{2+}-dependent phosphorylation of MLC. (For interpretation of the references to color in this figure legend, the reader is referred to the web version of this article at www.liebertonline.com/ars).

To investigate how activated G6PD is involved in modulating VSM contraction, we examined the effects of G6PD on the increase in $[Ca^{2+}]_i$ levels evoked by KCl-induced membrane depolarization, which predominantly enhances Ca^{2+} entry through voltage-operated Ca^{2+} channels and TRP channels (15, 41), or by U46619-induced GPCR activation, which increases Ca^{2+} entry through voltage-operated Ca^{2+} channels (52, 54). Our results provide novel evidence that increases in CASMC Ca^{2+} transients and a rise in global CA $[Ca^{2+}]_i$ evoked by KCl are significantly reduced by knocking down G6PD expression. Consistent with those findings, 6AN and 17-ketosteroids, which are competitive and uncompetitive inhibitors of G6PD, respectively, are known to attenuate the rise in $[Ca^{2+}]_i$ elicited by KCl and decrease chronic hypoxia-induced pulmonary vasoconstriction and pulmonary hypertension (5, 15, 19). We previously reported that modulation of G6PD by hypoxia regulates $[Ca^{2+}]_i$ and enhances pulmonary artery constriction and CA relaxation (19, 20, 23). We also observed that G6PD knockdown significantly reduced MYPT1 and MLC phosphorylation and extracellular Ca^{2+}-dependent CA contractions. This suggests that G6PD or G6PD-derived NADPH redox modulates CA contraction by increasing $[Ca^{2+}]_i$ through Ca^{2+} influx, which in turn activates Ca^{2+}-dependent MYPT1 and MLC kinase. These two enzymes are activated *via* Rho kinase and CaM kinase II signaling pathways, respectively, which are stimulated by KCl and U46619 in Ca^{2+}- and redox-dependent manner (17, 44, 51, 52). There are multiple redox-sensitive targets in VSM cells, including voltage-gated K^+ (K_v) and Ca^{2+} channels, and ryanodine receptors (24). In CASMCs and other cell types, NADPH oxido-reductases are known to regulate K_v channel and ryanodine receptor function and to trigger Ca^{2+} release from ryanodine-sensitive stores, leading to an increase in $[Ca^{2+}]_i$ (2, 55). It is therefore plausible that increases in G6PD-derived NADPH redox are involved in regulating KCl-induced activation of Ca^{2+} entry through voltage-sensitive Ca^{2+} channels or Ca^{2+}-induced Ca^{2+} release in VSM. For example, NADPH redox could regulate ion channel function by (i) directly binding to the Ca^{2+} channel proteins such as, the pore forming subunit of L-type Ca^{2+} channel, that contains pyridine binding sites, (ii) modulating the activity of oxido-reductases like thioredoxin or glutathione reductases that could modify several thiol residues in Ca^{2+} channel protein, and (iii) regulating NADPH oxidase-derived ROS generation that could increase $[Ca^{2+}]_i$ directly by activating L-type Ca^{2+} channels through oxidizing the key thiol groups in the pore forming S4 transmembrane loop or indirectly by activating Ca^{2+}-dependent CaM Kinase II, which is known to increase L-type Ca^{2+} channel function (17, 50, 53). In lieu of this notion, we found that silencing of G6PD significantly decreased ROS generation without altering glutathione reductase activity in CAs and attenuated KCl-induced CA contraction. Although precisely how activation of G6PD and increases in NADPH regulate Ca^{2+} influx and/or release remains unclear, our present findings imply that G6PD and the NADPH redox state are novel modulators of EC coupling, and that they contribute significantly to the regulation of vasomotor function, perhaps impacting diseases such as hypertension, CA disease, and diabetes-associated vasculopathies.

Studies in Mediterranean and Sardinian $G6PD^{def}$ individuals indicate that G6PD deficiency reduces the risk of cardiovascular diseases in $G6PD^{def}$ individuals (45). Although these studies suggest the possibility that G6PD deficiency confers protection against vascular disease, how it protects the cardiovascular system is poorly understood. Matsui *et al.* demonstrated that G6PD-derived NAPDH enhances superoxide anion generation, which mediates Ang II–induced hypertension and hypertrophy of smooth muscle (33). They also reported that superoxide levels and atherosclerotic lesions are considerably reduced by crossbreeding $ApoE^{-/-}$ and $G6PD^{-def}$ mice (34). Conversely, other studies have shown that G6PD is overexpressed in the stromal-vascular cells of diabetic *db/db* mice and, in the aortas of Zucker diabetic fatty rats, exacerbates oxidative stress, leading to vascular dysfunction (37, 46). Taken together, our present findings and those of Matsui *et al.* (33) suggest that increases in G6PD activity and elevated intracellular NADPH levels contribute to the development of coronary dysfunction and disease by acutely potentiating membrane depolarization-evoked and receptor-mediated smooth muscle contraction, increasing vasoconstriction, and evoking chronic remodeling of the vessel wall. G6PD deficiency presumably reduces functional changes in smooth muscle, thereby protecting individuals from vascular diseases by reducing pressure and/or shear stress on the vessel wall, and by reducing structural remodeling evoked by oxidative stress (33, 39).

Acknowledgments

Some of these data were presented at the AHA Scientific Session, Orlando, FL, 2007, and an abstract was published in

Circulation, 116 (16), II–204, 2007. This study was supported by grants from the AHA (#0435070N) and NIH (RO1HL085352). The authors are grateful to Drs. Jane Leopold and Joseph Loscalzo, Department of Medicine, Brigham and Women's Hospital and Harvard Medical School, Boston, MA 02115, for kindly providing $G6PD^{def}$ mice and for their valuable suggestions to improve this article.

Author Disclosure Statement

No competing financial interests exist.

References

1. Akaike N and Harata N. Nystatin perforated patch recording and its applications to analyses of intracellular mechanisms. *Jpn J Physiol* 44: 433–473, 1994.
2. Baker ML, Serysheva, II, Sencer S, Wu Y, Ludtke SJ, Jiang W, Hamilton SL, and Chiu W. The skeletal muscle Ca^{2+} release channel has an oxidoreductase-like domain. *Proc Natl Acad Sci U S A* 99: 12155–12160, 2002.
3. Barron JT, Glonek T, and Messer JV. 31P-nuclear magnetic resonance analysis of extracts of vascular smooth muscle. *Atherosclerosis* 59: 57–62, 1986.
4. Barron JT, Gu L, and Parrillo JE. Cytoplasmic redox potential affects energetics and contractile reactivity of vascular smooth muscle. *J Mol Cell Cardiol* 29: 2225–2232, 1997.
5. Bonnet S, Dumas-de-La-Roque E, Begueret H, Marthan R, Fayon M, Dos Santos P, Savineau JP, and Baulieu EE. Dehydroepiandrosterone (DHEA) prevents and reverses chronic hypoxic pulmonary hypertension. *Proc Natl Acad Sci U S A* 100: 9488–9493, 2003.
6. Burnashev N, Zhou Z, Neher E, and Sakmann B. Fractional calcium currents through recombinant GluR channels of the NMDA, AMPA and kainate receptor subtypes. *J Physiol* 485 (Pt 2): 403–418, 1995.
7. Cocco P, Todde P, Fornera S, Manca MB, Manca P, and Sias AR. Mortality in a cohort of men expressing the glucose-6-phosphate dehydrogenase deficiency. *Blood* 91: 706–709, 1998.
8. Eggleston LV and Krebs HA. Regulation of the pentose phosphate cycle. *Biochem J* 138: 425–435, 1974.
9. Gaskin RS, Estwick D, and Peddi R. G6PD deficiency: its role in the high prevalence of hypertension and diabetes mellitus. *Ethn Dis* 11: 749–754, 2001.
10. Gollasch M, Ried C, Liebold M, Haller H, Hofmann F, and Luft FC. High permeation of L-type Ca^{2+} channels at physiological [Ca^{2+}]: homogeneity and dependence on the alpha 1-subunit. *Am J Physiol* 271: C842–C850, 1996.
11. Gschwendt M, Muller HJ, Kielbassa K, Zang R, Kittstein W, Rincke G, and Marks F. Rottlerin, a novel protein kinase inhibitor. *Biochem Biophys Res Commun* 199: 93–98, 1994.
12. Gupte RS, Pozarowski P, Grabarek J, Traganos F, Darzynkiewicz Z, and Lee MY. RIalpha influences cellular proliferation in cancer cells by transporting RFC40 into the nucleus. *Cancer Biol Ther* 4: 429–437, 2005.
13. Gupte RS, Rawat DK, Chettimada S, Cioffi DL, Wolin MS, Gerthoffer WT, McMurtry IF, and Gupte SA. Activation of glucose-6-phosphate dehydrogenase promotes acute hypoxic pulmonary artery contraction. *J Biol Chem* 285: 19561–19571, 2010.
14. Gupte RS, Vijay V, Marks B, Levine RJ, Sabbah HN, Wolin MS, Recchia FA, and Gupte SA. Upregulation of glucose-6-phosphate dehydrogenase and NAD(P)H oxidase activity increases oxidative stress in failing human heart. *J Card Fail* 13: 497–506, 2007.
15. Gupte SA, Arshad M, Viola S, Kaminski PM, Ungvari Z, Rabbani G, Koller A, and Wolin MS. Pentose phosphate pathway coordinates multiple redox-controlled relaxing mechanisms in bovine coronary arteries. *Am J Physiol Heart Circ Physiol* 285: H2316–H2326, 2003.
16. Gupte SA, Kaminski PM, Floyd B, Agarwal R, Ali N, Ahmad M, Edwards J, and Wolin MS. Cytosolic NADPH may regulate differences in basal Nox oxidase-derived superoxide generation in bovine coronary and pulmonary arteries. *Am J Physiol Heart Circ Physiol* 288: H13–H21, 2005.
17. Gupte SA, Kaminski PM, George S, Kouznestova L, Olson SC, Mathew R, Hintze TH, and Wolin MS. Peroxide generation by p47phox-Src activation of Nox2 has a key role in protein kinase C-induced arterial smooth muscle contraction. *Am J Physiol Heart Circ Physiol* 296: H1048–H1057, 2009.
18. Gupte SA, Levine RJ, Gupte RS, Young ME, Lionetti V, Labinskyy V, Floyd BC, Ojaimi C, Bellomo M, Wolin MS, and Recchia FA. Glucose-6-phosphate dehydrogenase-derived NADPH fuels superoxide production in the failing heart. *J Mol Cell Cardiol* 41: 340–349, 2006.
19. Gupte SA, Li KX, Okada T, Sato K, and Oka M. Inhibitors of pentose phosphate pathway cause vasodilation: involvement of voltage-gated potassium channels. *J Pharmacol Exp Ther* 301: 299–305, 2002.
20. Gupte SA, Okada T, McMurtry IF, and Oka M. Role of pentose phosphate pathway-derived NADPH in hypoxic pulmonary vasoconstriction. *Pulm Pharmacol Ther* 19: 303–309, 2006.
21. Gupte SA, Rupawalla T, Phillibert D, Jr., and Wolin MS. NADPH and heme redox modulate pulmonary artery relaxation and guanylate cyclase activation by NO. *Am J Physiol* 277: L1124–L1132, 1999.
22. Gupte SA, Tateyama M, Okada T, Oka M, and Ochi R. Epiandrosterone, a metabolite of testosterone precursor, blocks L-type calcium channels of ventricular myocytes and inhibits myocardial contractility. *J Mol Cell Cardiol* 34: 679–688, 2002.
23. Gupte SA and Wolin MS. Hypoxia promotes relaxation of bovine coronary arteries through lowering cytosolic NADPH. *Am J Physiol Heart Circ Physiol* 290: H2228–H2238, 2006.
24. Gupte SA and Wolin MS. Oxidant and redox signaling in vascular oxygen sensing: implications for systemic and pulmonary hypertension. *Antioxid Redox Signal* 10: 1137–1152, 2008.
25. Jones ML, Craik JD, Gibbins JM, and Poole AW. Regulation of SHP-1 tyrosine phosphatase in human platelets by serine phosphorylation at its C terminus. *J Biol Chem* 279: 40475–40483, 2004.
26. Kauffman FC, Brown JG, Passonneau JV, and Lowry OH. Effects of changes in brain metabolism on levels of pentose phosphate pathway intermediates. *J Biol Chem* 244: 3647–3653, 1969.
27. Kim JY and Saffen D. Activation of M1 muscarinic acetylcholine receptors stimulates the formation of a multiprotein complex centered on TRPC6 channels. *J Biol Chem* 280: 32035–32047, 2005.
28. Ledoux J, Taylor MS, Bonev AD, Hannah RM, Solodushko V, Shui B, Tallini Y, Kotlikoff MI, and Nelson MT. Functional architecture of inositol 1,4,5-trisphosphate signaling in restricted spaces of myoendothelial projections. *Proc Natl Acad Sci U S A* 105: 9627–9632, 2008.
29. Leopold JA, Cap A, Scribner AW, Stanton RC, and Loscalzo J. Glucose-6-phosphate dehydrogenase deficiency promotes endothelial oxidant stress and decreases endothelial nitric oxide bioavailability. *FASEB J* 15: 1771–1773, 2001.

30. Leopold JA, Walker J, Scribner AW, Voetsch B, Zhang YY, Loscalzo AJ, Stanton RC, and Loscalzo J. Glucose-6-phosphate dehydrogenase modulates vascular endothelial growth factor-mediated angiogenesis. *J Biol Chem* 278: 32100–32106, 2003.
31. Leopold JA, Zhang YY, Scribner AW, Stanton RC, and Loscalzo J. Glucose-6-phosphate dehydrogenase overexpression decreases endothelial cell oxidant stress and increases bioavailable nitric oxide. *Arterioscler Thromb Vasc Biol* 23: 411–417, 2003.
32. Maasch C, Wagner S, Lindschau C, Alexander G, Buchner K, Gollasch M, Luft FC, and Haller H. Protein kinase calpha targeting is regulated by temporal and spatial changes in intracellular free calcium concentration [$Ca^{(2+)}$](i). *FASEB J* 14: 1653–1663, 2000.
33. Matsui R, Xu S, Maitland KA, Hayes A, Leopold JA, Handy DE, Loscalzo J, and Cohen RA. Glucose-6 phosphate dehydrogenase deficiency decreases the vascular response to angiotensin II. *Circulation* 112: 257–263, 2005.
34. Matsui R, Xu S, Maitland KA, Mastroianni R, Leopold JA, Handy DE, Loscalzo J, and Cohen RA. Glucose-6-phosphate dehydrogenase deficiency decreases vascular superoxide and atherosclerotic lesions in apolipoprotein E(−/−) mice. *Arterioscler Thromb Vasc Biol* 26: 910–916, 2006.
35. Murata Y, Iwasaki H, Sasaki M, Inaba K, and Okamura Y. Phosphoinositide phosphatase activity coupled to an intrinsic voltage sensor. *Nature* 435: 1239–1243, 2005.
36. Ozaki H, Gerthoffer WT, Publicover NG, Fusetani N, and Sanders KM. Time-dependent changes in Ca^{2+} sensitivity during phasic contraction of canine antral smooth muscle. *J Physiol* 440: 207–224, 1991.
37. Park J, Choe SS, Choi AH, Kim KH, Yoon MJ, Suganami T, Ogawa Y, and Kim JB. Increase in glucose-6-phosphate dehydrogenase in adipocytes stimulates oxidative stress and inflammatory signals. *Diabetes* 55: 2939–2949, 2006.
38. Pinna A, Carru C, Solinas G, Zinellu A, and Carta F. Glucose-6-phosphate dehydrogenase deficiency in retinal vein occlusion. *Invest Ophthalmol Vis Sci* 48: 2747–2752, 2007.
39. Pinna A, Solinas G, Masia C, Zinellu A, Carru C, and Carta A. Glucose-6-phosphate dehydrogenase (G6PD) deficiency in nonarteritic anterior ischemic optic neuropathy in a Sardinian population, Italy. *Invest Ophthalmol Vis Sci* 49: 1328–1332, 2008.
40. Rajasekaran NS, Connell P, Christians ES, Yan LJ, Taylor RP, Orosz A, Zhang XQ, Stevenson TJ, Peshock RM, Leopold JA, Barry WH, Loscalzo J, Odelberg SJ, and Benjamin IJ. Human alpha B-crystallin mutation causes oxido-reductive stress and protein aggregation cardiomyopathy in mice. *Cell* 130: 427–439, 2007.
41. Ratz PH and Berg KM. 2-Aminoethoxydiphenyl borate inhibits KCl-induced vascular smooth muscle contraction. *Eur J Pharmacol* 541: 177–183, 2006.
42. Ratz PH, Miner AS, and Barbour SE. Calcium-independent phospholipase A2 participates in KCl-induced calcium sensitization of vascular smooth muscle. *Cell Calcium* 46: 65–72, 2009.
43. Recchia FA, Osorio JC, Chandler MP, Xu X, Panchal AR, Lopaschuk GD, Hintze TH, and Stanley WC. Reduced synthesis of NO causes marked alterations in myocardial substrate metabolism in conscious dogs. *Am J Physiol Endocrinol Metab* 282: E197–E206, 2002.
44. Rokolya A and Singer HA. Inhibition of CaM kinase II activation and force maintenance by KN-93 in arterial smooth muscle. *Am J Physiol Cell Physiol* 278: C537–C545, 2000.
45. Sanna F, Bonatesta RR, Frongia B, Uda S, Banni S, Melis MP, Collu M, Madeddu C, Serpe R, Puddu S, Porcu G, Dessi S, and Batetta B. Production of inflammatory molecules in peripheral blood mononuclear cells from severely glucose-6-phosphate dehydrogenase-deficient subjects. *J Vasc Res* 44: 253–263, 2007.
46. Serpillon S, Floyd BC, Gupte RS, George S, Kozicky M, Neito V, Recchia F, Stanley W, Wolin MS, and Gupte SA. Superoxide production by NAD(P)H oxidase and mitochondria is increased in genetically obese and hyperglycemic rat heart and aorta before the development of cardiac dysfunction. The role of glucose-6-phosphate dehydrogenase-derived NADPH. *Am J Physiol Heart Circ Physiol* 297: H153–H162, 2009.
47. Singer HA, Schworer CM, Sweeley C, and Benscoter H. Activation of protein kinase C isozymes by contractile stimuli in arterial smooth muscle. *Arch Biochem Biophys* 299: 320–329, 1992.
48. Smith JM, Paulson DJ, and Solar SM. $Na^{+}/K^{(+)}$-ATPase activity in vascular smooth muscle from streptozotocin diabetic rat. *Cardiovasc Res* 34: 137–144, 1997.
49. Somlyo AP and Somlyo AV. Signal transduction and regulation in smooth muscle. *Nature* 372: 231–236, 1994.
50. Trebak M, Ginnan R, Singer HA, and Jourd'heuil D. Interplay between calcium and reactive oxygen/nitrogen species: an essential paradigm for vascular smooth muscle signaling. *Antioxid Redox Signal* 12: 657–674, 2010.
51. Wang Y, Yoshioka K, Azam MA, Takuwa N, Sakurada S, Kayaba Y, Sugimoto N, Inoki I, Kimura T, Kuwaki T, and Takuwa Y. Class II phosphoinositide 3-kinase alpha-isoform regulates Rho, myosin phosphatase and contraction in vascular smooth muscle. *Biochem J* 394: 581–592, 2006.
52. Wilson DP, Susnjar M, Kiss E, Sutherland C, and Walsh MP. Thromboxane A2-induced contraction of rat caudal arterial smooth muscle involves activation of Ca^{2+} entry and Ca^{2+} sensitization: Rho-associated kinase-mediated phosphorylation of MYPT1 at Thr-855, but not Thr-697. *Biochem J* 389: 763–774, 2005.
53. Xie LH, Chen F, Karagueuzian HS, and Weiss JN. Oxidative-stress-induced afterdepolarizations and calmodulin kinase II signaling. *Circ Res* 104: 79–86, 2009.
54. Yamagishi T, Yanagisawa T, and Taira N. Ca^{2+} influx induced by the agonist U46619 is inhibited by hyperpolarization induced by the K+channel opener cromakalim in canine coronary artery. *Jpn J Pharmacol* 59: 291–299, 1992.
55. Yi XY, Li VX, Zhang F, Yi F, Matson DR, Jiang MT, and Li PL. Characteristics and actions of NAD(P)H oxidase on the sarcoplasmic reticulum of coronary artery smooth muscle. *Am J Physiol Heart Circ Physiol* 290: H1136–H1144, 2006.

Address correspondence to:
Dr. Sachin A. Gupte
Department of Biochemistry & Molecular Biology
MSB 2312, University of South Alabama
307 University Blvd.
Mobile, AL 36688

E-mail: sagupte@usouthal.edu

Date of first submission to ARS Central, March 23, 2010; date of final revised submission, July 20, 2010; date of acceptance, July 21, 2010.

Abbreviations Used

AMPB = amphotericin B
Ang II = angiotensin II
BCA = bovine coronary artery
BF = bright field
CA = coronary artery
cGFP = coral green fluorescent protein
DHE = dihydroeithidium
DMEM = Dulbecco's modified Eagle's medium
EC = excitation–contraction
EGTA = ethylene glycol tetraacetic acid
G6PD = glucose-6-phosphate dehydrogenase
$G6PD^{def}$ = glucose-6-phosphate dehydrogenase deficient
G6PD-RFP-S = glucose-6-phosphate dehydrogenase-Red fluorescence protein—S210A mutant
G6PD-RFP-T = glucose-6-phosphate dehydrogenase-Red fluorescence protein—T266A mutant
G6PD-RFP-wt = glucose-6-phosphate dehydrogenase-Red fluorescence protein—wild type
GPCR = G protein-coupled receptor
HEPES = 1-piperazineethanesulfonic acid
HSP20 = heat-shock protein 20
KCl = potassium chloride
MLC = myosin light chain
MYPT1 = myosin phosphatase target subunit 1
NADPH = nicotinamide adenine dinucleotide phosphate reduced
NO = nitric oxide
NT = nontargeting
PBS = phosphate-buffered saline
PDBu = phorbol 12, 13-dibutyrate
PKC = protein kinase C
PPP = pentose phosphate pathway
ROS = reactive oxygen species
SDS = sodium dodecyl sulfate
SMC = smooth muscle cell
U46619 = 15(*S*)-hydroxy-11,9-(epoxy-methano)prostadienoic acid
UT = untransfected
VSM = vascular smooth muscle